Chapter 3

Doubly excited resonances of helium

By absorbing one photon, one can reach from ground-state of helium a final state with one electron in the continuum and the second one in the ground or excited state of the remaining ion. These final states can be reached via two different paths as shown in Fig. 3.1. The first path is the direct photoionization channel with excitation, i.e. one electron is promoted to the continuum and the second one is excited to a higher orbit. This process can be described by

$$\mathrm{He}(1s^2)\ {}^1S^e + h\nu \rightarrow [\mathrm{He}^+(nl) + e^-]\ {}^1P^o. \tag{3.1}$$

Here n and l are principal quantum number and orbital angular momentum quantum number, respectively. In the second path, both electrons are first excited to a discrete state, which subsequently decays via autoionization. This process can be described by

$$\mathrm{He}(1s^2)\ {}^1S^e + h\nu \ \ \rightarrow \ \ \mathrm{He}^*(N, K_{n'})\ {}^1P^o \rightarrow [\mathrm{He}^+(nl) + e^-]\ {}^1P^o, \tag{3.2}$$

where $N, K_{n'}$ is a simplified classification scheme. N, n', and K are approximate radial and angular quantum numbers, respectively; and a detailed discussion will be given

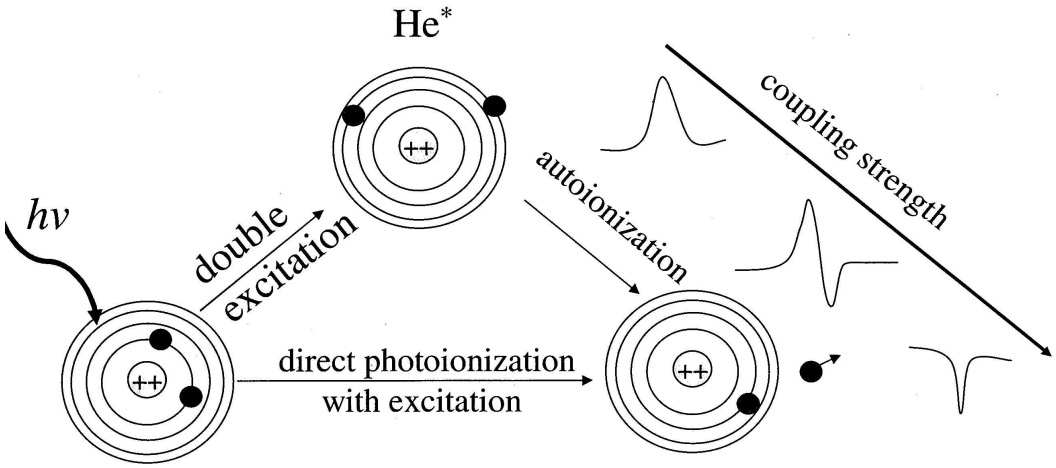

Figure 3.1: Schematic representation of photoionization following excitation from the ${}^1S^e$ ground state of helium to a ${}^1P^o$ final state.

in Sect. 3.2. In the energy domain, these two processes cannot be distinguished by experiment and, therefore, according to the interference of these two decay paths, Fano profiles are observed in the spectra. Three different cases (weak, medium, and strong) for the dependence of the lineshape of the resonance on the coupling strength are shown in Fig. 3.1, that will be discussed together with the Fano parameter q in Sect. 3.1.1. The two paths mentioned occur on different time scales and one can distinguish them in the time domain. Sub-fs extreme ultraviolet pulses and attosecond streaking techniques can trace the buildup of a Fano resonance in the time domain; the feasibility of such experiments has been analyzed theoretically [56].

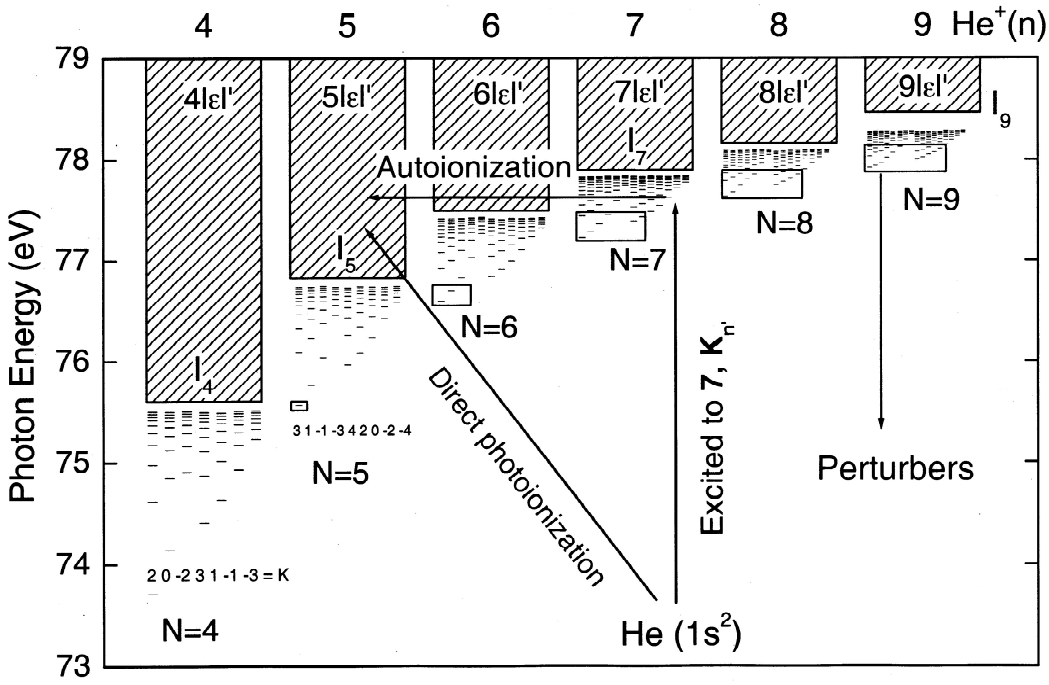

Figure 3.2: Energy diagram of the $^1P^o$ double-excitation resonances below the SITs I_4 to I_9 in He with energies taken from Ref. [31]. $2N-1$ Rydberg series indicated by some horizontal lines are converged to single ionization threshold (SIT) I_N. The lines with arrows represent different paths which lead to the final continuum states with the remaining electron in $\mathrm{He}^+(n = 1, \cdots, 6)$. The resonances in the boxes are the perturbers.

Fig. 3.2 shows the energy level scheme of double-excitation resonances in helium below the single ionization thresholds (SIT) I_4 to I_9. Two different paths leading to the final continuum states, namely autoionization and direct photoionization with excitation, are indicated in this figure; they were discussed above, see Fig. 3.1. As marked on the upper x-axis in this figure, the doubly excited states $N, K_{n'}$ $(N = 7)$ can decay to the final continuum states with the remaining electron in the He^+(n) states with $n = 1$ to 6. Observably $N-1$ channels with $n = 1$ to $N-1$ are open if one scans spectra at photon energies between I_{N-1} and I_N, i.e. in this energy region $N-1$ satellites can be resolvable from channel-resolved measurements such as experimental PCSs. These different decay channels can be distinguished by the kinetic energies of the corresponding photoelectrons

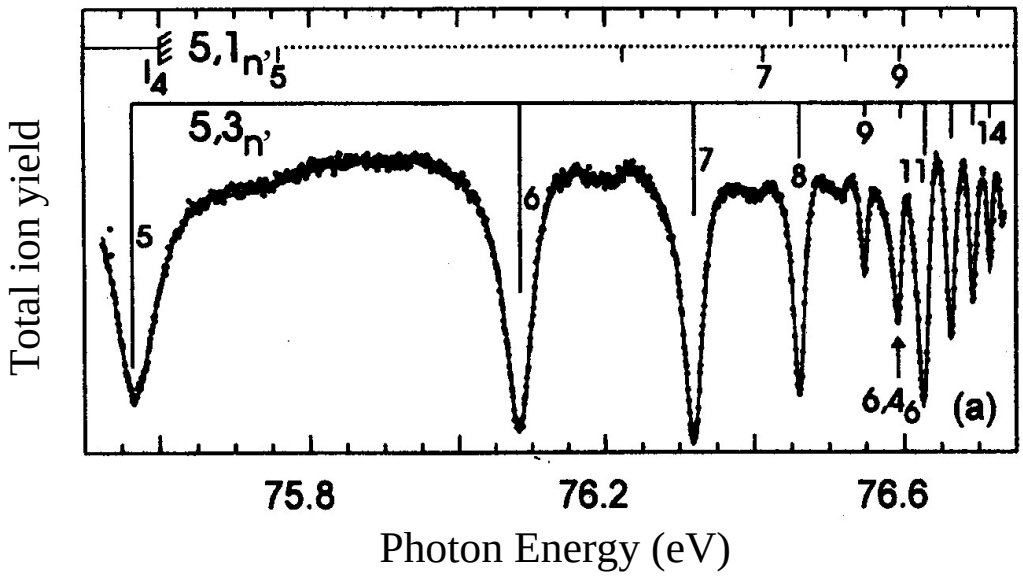

Figure 3.3: Experimental total cross sections below the SIT I_6. The position of the perturber $6, 4_6$ is indicated by an arrow. The figure is taken from Ref. [30]

.

that correspond to the PCSs, σ_n.

The most interesting feature is the occurrence of perturbers, which are indicated by boxes in Fig. 3.2. Perturbers are low-lying resonances of a Rydberg series below I_N that lie energetically in the region of high-lying resonances below I_{N-1}. Figure 3.2 displays the first perturber located exactly at I_4, but more and more perturbers appear in the Rydberg series below higher single-ionization thresholds. The appearance of perturber states dramatically modulates Fano profiles of resonances that converge towards a lower ionization threshold. Total cross sections below the SIT I_6 given in Fig. 3.3, as an example, show how the spectrum is affected by the perturber $6, 4_6$, which is indicated by a vertical arrow. Clearly, in the region of the perturber, the resonances of Rydberg series $5, 3_{n'}$ are significantly varied. In this dissertation, we are concerned with the energy region above the SIT I_8, where a large number of perturbers cause the spectra to fluctuate and to become complicated. Therefore, one expects to observe Ericson fluctuations [26] in the spectra, which describes the fact that it is impossible to identify each resonance due to strong overlaps of the states. Ericson fluctuations, originally observed in nuclear physics, have become quantum signatures of chaos in atomic system (discussed later).

3.1 Parameterizations of resonance profiles in cross sections

In principle, one can calculate cross sections and ADPs with Eq. (1.23) and Eq. (1.24), but these complicated formula cannot be used directly for the analysis of experimental

data. Therefore, a parameterization of resonance profiles can clarify the physical picture of a resonance and allows one to perform a more quantitative comparison between experimental results and calculations. In the following subsections, we shall discuss the parameterizations of resonance profiles in the TCS, the PCS, and the ADP, that will be used in the fit analysis of our data.

3.1.1 Fano profiles for the total cross sections

The resonances in the absorption spectra exhibit pronounced Fano profiles that originate from an interference between direct photoionization and indirect photoionization channels as discussed before. This leads to Fano profiles of the form [20, 57]:

$$\sigma_T(E) = \sigma_a \frac{(q+\epsilon)^2}{1+\epsilon^2} + \sigma_b, \text{ with reduced energy } \epsilon = 2\frac{E-E_r}{\Gamma}. \tag{3.3}$$

Here, E_r is the resonance energy and Γ the natural width given by the decay rate of the autoionization resonance. The Fano parameter q represents the discrete/continuum mixing strength, i.e. coupling strength. With $|i\rangle$, $|\nu\rangle$, and $|f\rangle$ describing the initial, intermediate (discrete state), and final continuum state, respectively, the linewidth can be written as

$$\Gamma = 2\pi \left|\langle f|V|\nu\rangle\right|^2, \tag{3.4}$$

where V represents the Coulomb interaction. σ_a and σ_b represent the non-resonant background cross sections for transitions to continuum states that interact or do not interact, respectively, with discrete autoionization states [57]. Therefore, σ_a is affected by the interaction whereas σ_b is constant. The Fano parameter q is given by

$$q = \frac{\langle \nu|r|i\rangle}{\pi\langle \nu|V|f\rangle\langle f|r|i\rangle}, \tag{3.5}$$

which represents the ratio of the dipole matrix element of a transition to a discrete state to that of a transition to the continuum, which interacts with the discrete state. As demonstrated in Fig. 3.1, for the case that the coupling strength between the final state $|f\rangle$ and the discrete state $|\nu\rangle$ is very weak, the value for q in Eq. 3.5 becomes large and a Lorentz lineshape is observed in the cross section; for a strong coupling strength, q is close to zero and one can see a window dip; for all other cases of the coupling strength, the variation in the cross section caused by a resonance is described by a Fano-like lineshape. If q is negative, the minimum in the absorption cross section occurs on the high-energy side of the line and otherwise on the low-energy side, as can be seen in Fig. 3.4 by the simulations to Eq. (3.3).

By setting $\sigma_a/(\sigma_a+\sigma_b) = \rho^2$ and $\sigma_T^0 = \sigma_a+\sigma_b$, the σ_T in Eq. (3.3) can also be written as [57, 58]

$$\sigma_T = \sigma_T^0 \left(\rho^2 \frac{(q+\epsilon)^2}{1+\epsilon^2} + 1 - \rho^2\right). \tag{3.6}$$

Here, ρ^2 is the fractional part of the TCS that interacts with the resonance [58] and it is called correlation parameter. σ_T^0 represents the off-resonance TCS.

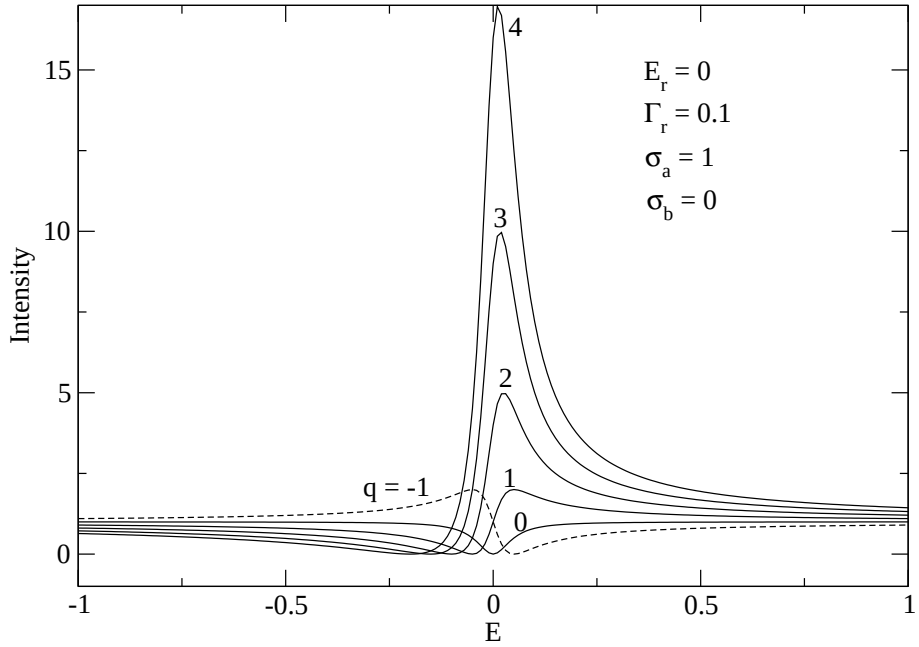

Figure 3.4: Simulations of Fano lineshapes as a function of q for various values of $q = -1$, 0, 1, 2, 3, and 4. The values of the other parameters used in the simulations are given in the figure.

3.1.2 Starace's formula for partial cross sections

In Ref. [59], Starace used the observed channels to describe the resonance profiles in the PCS. A PCS denoted by P can be described analytically by

$$\begin{aligned}\sigma_P &= \sigma_P^0 + \frac{\sigma_P^0}{1+\epsilon^2}\{2\epsilon(q\mathrm{Re}\langle\alpha\rangle_P - \mathrm{Im}\langle\alpha\rangle_P) \\ &\quad -2q\mathrm{Im}\langle\alpha\rangle_P - 2\mathrm{Re}\langle\alpha\rangle_P + (q^2+1)\langle|\alpha|^2\rangle_P\}. \end{aligned} \tag{3.7}$$

Here, σ_P^0 is the PCS in the absence of a resonance and the second term describes the Fano-like lineshape of the resonance in σ_P. α is the Starace parameter [59] and represents the fraction of the dipole amplitude. Setting $C_1 = q\mathrm{Re}\langle\alpha\rangle_P - \mathrm{Im}\langle\alpha\rangle_P$ and $C_2 = 1 - 2q\mathrm{Im}\langle\alpha\rangle_P - 2\mathrm{Re}\langle\alpha\rangle_P + (q^2+1)\langle|\alpha|^2\rangle_P$, the above equation can be written as

$$\sigma_P = \frac{\sigma_P^0}{1+\epsilon^2}\{\epsilon^2 + 2\epsilon C_1 + C_2\}. \tag{3.8}$$

This equation depends on only *two* independent linear combinations, C_1 and C_2, of the *three* parameters $\langle|\alpha|^2\rangle_P$, $\mathrm{Re}\langle\alpha\rangle_P$, and $\mathrm{Im}\langle\alpha\rangle_P$. As a consequence, one may only determine C_1 and C_2 by fitting Eq. (3.8) to the experimental data, but $\langle|\alpha|^2\rangle_P$, $\mathrm{Re}\langle\alpha\rangle_P$, and $\mathrm{Im}\langle\alpha\rangle_P$ cannot be determined from the fit. Interestingly, one may note that the formula for describing the resonances in the PCS given in Eq. (3.8) has the same mathematical structure as the Fano formula (Eqs. (3.3) and (3.6)) for the TCS. Therefore, it is possible to describe the PCSs by the Fano formula, but in this case q as well as C_1 and C_2 represent only effective parameters without deeper physical meaning. The relation between these parameters is [60]

$$C_1 = \rho^2(q^2-1) + 1 = \frac{\sigma_a q + \sigma_b}{\sigma_b}$$

$$\begin{aligned} C_2 &= 2q\rho^2 = \frac{\sigma_a}{\sigma_b} \\ \sigma_P^0 &= \frac{\sigma_T^0}{\rho^2} = \sigma_b. \end{aligned} \tag{3.9}$$

The Fano formula given in Eqs. (3.3) and (3.6), together with Eq. (3.8), can be used to fit the experimental TCSs or PCSs.

3.1.3 Kabachnik's formula for the angular distribution parameters

The transition matrix elements in Eq. (1.24), which characterize excitation and autoionization decay, have to be parameterized, so that they can be used in the fit analysis of the experimental data. To this purpose, Kabachnik [46] parameterized the ADPs β given in Eq. (1.22) in the following way:

$$\begin{aligned} \beta &= -2\frac{X\epsilon^2 + Y\epsilon + Z}{A\epsilon^2 + B\epsilon + C} \\ &= -2\frac{X}{A} \cdot \frac{\epsilon^2 + \frac{Y}{X}\epsilon + \frac{Z}{X}}{\epsilon^2 + \frac{B}{A}\epsilon + \frac{C}{A}}, \end{aligned} \tag{3.10}$$

with

$$\begin{aligned} A &= \frac{\sigma_a + \sigma_b}{4\pi} \\ B &= \frac{2q\sigma_a}{4\pi} \\ C &= \frac{\sigma_a q^2 + \sigma_b}{4\pi}. \end{aligned} \tag{3.11}$$

The parameters X, Y, and Z are related to the transition amplitudes and the phase shifts given in Eq. (49) in Ref. [46]. They are considered to be slowly varying functions of energy and may be regarded as correlation constants in the vicinity of a resonance. With the off-resonance value $\beta_0 = -2X/A$ and the relations given in Eq. (3.11), one can write Eq. (3.10) as

$$\beta = \beta_0 \frac{(\epsilon^2 + \frac{Y}{X}\epsilon + \frac{Z}{X})(\sigma_a + \sigma_b)}{\sigma_a(\epsilon + q)^2 + \sigma_b(\epsilon^2 + 1)}. \tag{3.12}$$

With the new parameters $F = Y/X$ and $G = Z/X$, Eq. (3.12) becomes

$$\begin{aligned} \beta &= \beta_0 \frac{\epsilon^2 + F\epsilon + G}{\sigma_T} \cdot \frac{\sigma_a + \sigma_b}{\epsilon^2 + 1} \\ &= \beta_0 \frac{\epsilon^2 + F\epsilon + G}{\rho^2(\epsilon + q)^2 + (1 - \rho^2)(\epsilon^2 + 1)}. \end{aligned} \tag{3.13}$$

In the measurements, PCSs together with other DCSs are measured, and these data are used to derive the corresponding ADPs. Due to possible fluctuations caused by other

DCSs, the PCSs become more reliable with respect to the ADP. Therefore, with Eq. 3.13, a parallel fit for β is recommended by sharing the two parameters q and ρ^2 with the PCS, but not F, G, and β_0. We shall apply this procedure to our ADP data in the near future.

One can also simply write the ADP in Eq. (3.10) as

$$\beta = \beta_0 \frac{\epsilon^2 + a_1\epsilon + b_1}{\epsilon^2 + a_2\epsilon + b_2}. \tag{3.14}$$

In this case, a_1, b_1, a_2, and b_2 can also be regarded as correlation constants in an isolated resonance. During a fit process, one has to take into account the conditions $b_2 = (q^2\sigma_a + \sigma_b)/(\sigma_a + \sigma_b) > 0$ and $a_2 = (2q\sigma_a)/(\sigma_a + \sigma_b)$. Indeed, according to the large number of parameters (5 independent parameters in addition to the Fano parameters q, Γ, and E_r) in Eq. (3.14), it is quite difficult to extract them correctly from a fit to experimental data, particularly in case of overlapping resonances. In the vicinity of a resonance, the terms in the numerator and denominator of Eq. (3.10) change differently, so that their extrema are at different excitation energies and, as a result, β can vary rapidly. From simulations performed with Eq. (3.14), the variations in β show strong dependence on the parameters in the denominator.

3.2 Classification schemes for doubly excited resonances of helium

In this dissertation, we introduce two different classification schemes to describe doubly excited resonances in helium. The first is based on a molecular adiabatic description of helium, which uses the quantum numbers n_λ, n_μ, and m. These quantum numbers are equivalent to the approximate quantum numbers $N(K,T)^A_{n'}$ which were derived from group theory by Herrick and Sinanoğlu [23, 61]. In this dissertation, both classification schemes will be employed to understand the dynamics of doubly excited resonances in a two-electron system. The transformations between molecular quantum numbers and Herrick's approximate quantum numbers will also be presented in this section.

3.2.1 Molecular adiabatic approximation

In order to fully understand the decay dynamics of doubly excited states, Feagin and Briggs [24] introduced in 1986 an adiabatic approximations similar to the Born-Oppenheimer approximation for H_2^+, but with a reversed role of electrons and nuclei (see Fig. (3.5)).

The most important feature of the molecular adiabatic approximation is the fact that the two-center Hamiltonian is separable in prolate spheroidal coordinates that are plotted in Fig. 3.6. In this case, individual resonances are obtained by calculating vibrational eigenstates according to the Schrödinger equation,

$$\left(-\frac{\partial^2}{\partial R^2} + V_{n_\lambda, n_\mu, m} - E_{n'}\right) f_{n'}(R) = 0, \tag{3.15}$$

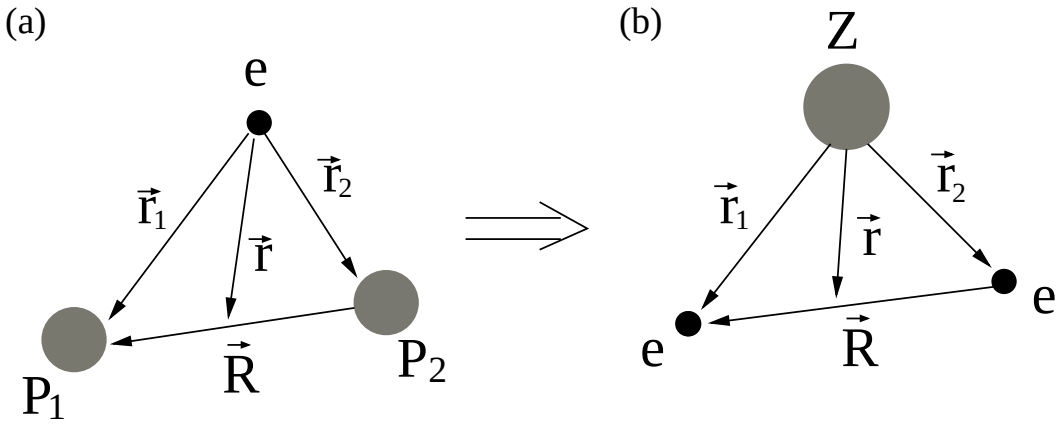

Figure 3.5: (a) Schematic of H_2^+ and (b) of the helium atom with reversed roles for the electrons and nucleus. $\vec{r}_1$ and $\vec{r}_2$ are the two possible distances between electrons and nuclei. $\vec{r}$ is the distance between electron (nucleus) and the center of two nuclei (electrons). P and e represent the proton and electron, respectively, and $\vec{R}$ is the distances between the two identical particles.

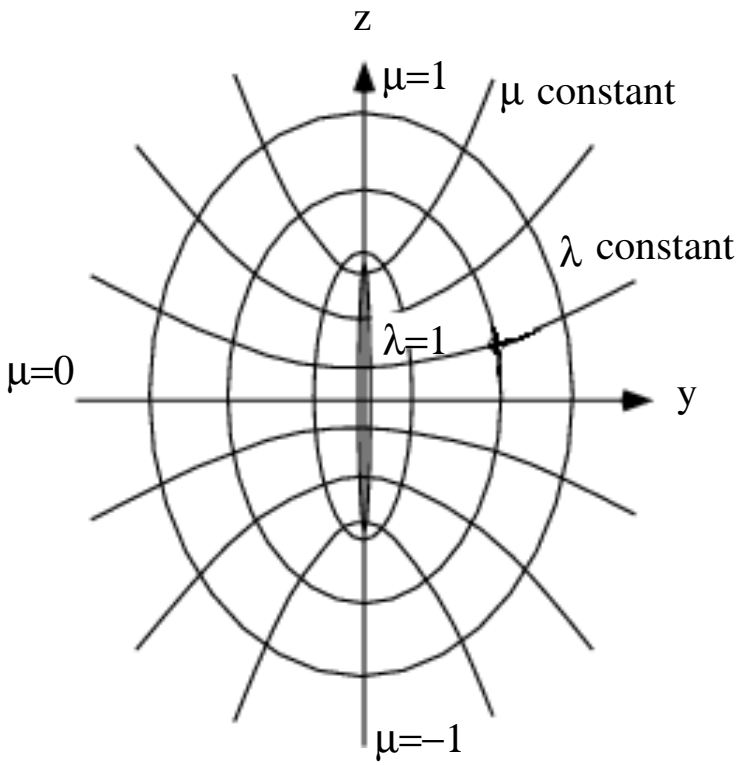

Figure 3.6: Schematic of the prolate coordinates λ and μ.

where R is the distance between the two identical particles, i.e. the electrons in case of helium. The quantum numbers n_λ and n_μ count the nodes along the respective coordinates λ and μ. m is the angular quantum number corresponding to the rotation angle along the Z axis in Fig. 3.6. The potentials $V_{n_\lambda,n_\mu,m}$ lead to a set of adiabatic avoided-crossing potential curves, which represent Rydberg series. n' are vibrational energies in these potential curves, but in doubly excited states they specify the excitation

of one electron to a Rydberg series, i.e. they represent the index of a Rydberg series. So far, a complete classification of doubly excited state can be described by quantum numbers n_λ, n_μ, m, and n'.

3.2.2 Herrick's classification schemes

The classification scheme $N(K,T)^A_{n'}$ [23, 61], which is identical to the molecular scheme with quantum numbers n_λ, n_μ, and m, is often employed to identify an isolated doubly excited resonance with N and n', respectively, standing for the ionization threshold of a given channel and the running index of the considered Rydberg series. In an independent particle picture, $N(n')$ may be understood as the principal quantum number of the inner (outer) electron; K is one of the angular-correlation quantum numbers and proportional to the average value of $r_1 cos\theta_{12}$, where r_1 refers to the inner electron and θ_{12} is the angle between the two electrons. T, the second angular-correlation quantum number, represents the relative orientation between the orbitals of the two electrons, which is equivalent to quantum number m in molecular approximation. A is called the radial correlation quantum number, which reflects a symmetry (the wave function of $A = +1$ states has an antinode and $A = -1$ states with a node) with respect to the x-y-plane ($\mu = 0$, i.e. $r_1 = r_2$) in Fig. 3.6. Close to the double-ionization threshold (N and n' are quite large), one obtains

$$K \rightarrow -N\langle cos\theta_{12}\rangle \tag{3.16}$$

from

$$\langle cos\theta_{12}\rangle \rightarrow -\frac{K}{N} + \frac{N^2 - 1 + K^2 - T^2 + 2ll'}{2Nn'}, \tag{3.17}$$

where l (l') is the orbital angular quantum number for the inner (outer) electron, respectively. For a given L and N, the ranges for K and T are given as follows [23]:

$$\begin{aligned} T &= 0, 1, \cdots, \min(L, N-1), \\ \pm K &= N - T - 1, N - T - 3, \cdots, 1(\text{or } 0). \end{aligned} \tag{3.18}$$

For $^1P^o$ double-excitation resonance of helium, T is limited to 1 and 0 and K has $2N-1$ values below a given ionization threshold I_N. $N, K = N - 2$ is the principal Rydberg series, which carries most intensity in the spectra, with resonances that have larger line widths.

Herrick's quantum numbers $N(K,T)^A_{n'}$ correspond to the molecular quantum numbers $[n_\lambda n_\mu m]_{n'}$ by the following relations:

$$\begin{array}{lcl} \text{molecular} & & \text{Herrick} \\ n_\lambda & = & \frac{1}{2}(N - K - 1 - T) \\ [n_\mu/2] & = & \frac{1}{2}(N + K - 1 - T) \\ m & = & T \\ (-1)^{n_\mu} & (=) & A. \end{array} \tag{3.19}$$

Here, $N = n_\lambda + [n_\mu/2] + m + 1$ and $K = n_\lambda - [n_\mu/2]$. The notation $[n_\mu/2]$ stands for the closest integer lower than $n_\mu/2$; In the two-center adiabatic approach, the fact that $A = 0$ does not occur is implied in the last equality in parentheses of Eq. (3.19) (for details see Ref. [31]). The approximate quantum numbers $[n_\lambda n_\mu m]_{n'}$ and $N(K,T)^A_{n'}$ imply the nodal structure of the wave function, which in turn leads to the propensity rules of radiative and non-radiative transitions (see Sect. 5.3.2).